PIV measurements in viscoelastic polyacrylamide solution in Taylor-Couette system

M. Smieszek[1], N. Abcha[2], I. Mutabazi[2] C. Egbers[1]
[1] Lehrstuhl für Aerodynamik und Strömungslehre (LAS),
Brandenburgische Technische Universität Cottbus, Siemens-Halske-Ring 14
03046 Cottbus
[2] Laboratoire de Mécanique, Physique et Géosciences (LMPG),
Université du Havre, 25, rue Philippe Lebon, BP 540
76058 Le Havre Cedex, France
smieszm@tu-cottbus.de http://www.tu-cottbus.de/LAS

Abstract

Particle image velocimetry is used to investigate the local velocity fields in Taylor-Couette system with viscoelastic polyacrylamide solution. We present results measured at different positions in small and large aspect ratio Taylor-Couette systems to investigate different boundary influence on flow stability. Experimental investigations in large aspect ratio Taylor-Couette system are done in LMPG at Université du Havre. The small system is used in LAS at BTU Cottbus. The experimental results are analysed with spectral methods to obtain spatial and temporal properties.

1 Introduction

Non-Newtonian fluids are wiedely used in industrial applications like food processing or polymer industry. It is of great interest to determine instability conditions, the efficience of transport and mixing of such materials. The complex rheological behaviour of non-Newtonian fluids can leads to unrequested phenomena like rod-climbing (Weissenberg effect), demixing or die swelling [1].
Adrian [3] gives a review about PIV. It is also discussed issues related to particle size, seeding density, illumination, image recording and interrogation. Pakdel and Mckinley [2] used PIV to measure the velocity of viscoelastic fluids in circular pipes, lid-driven cavity and time-dependent free surface extensional flow in a liquid filament. Baumert and Muller [4] reported results of PIV in weak, viscoelastic Taylor-Couette flow using long exposure times.

2 Experimental setup

The Taylor-Couette system, schematically shown in figure 1, consists of two concentric cylinders with the radius r_i and r_a and the legth L. Hence one defines the radius ratio

$\eta = r_i/r_a$ and the aspect ratio as $\Gamma = L/d$. $d = r_a - r_i$ as gap width. The inner cylinder rotates with the angular velocity Ω_i, the outer one is at rest.

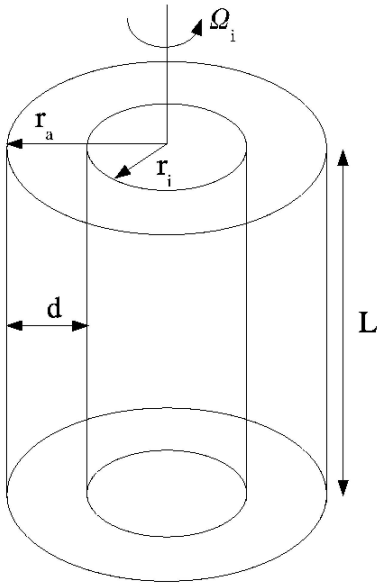

Figure 1: Schematic representation of the Taylor-Couette system.

We use two different Taylor-Couette systems with different geometric parameters. The first one has a length of $L = 459mm$. The inner cylinder has a radius of $r_i = 40mm$, the outer one $r_a = 50mm$ ($\eta = 0.8$ and $\Gamma = 45.9$). The geometric parameters of the second system are as follows: the inner cylinder has a diameter of $r_i = 25mm$, the outer one $r_a = 50mm$ and the length $L = 250mm$ ($\eta = 0.5$ and $\Gamma = 10$).

Experiment Fluid

A solution of 65% saccharose and 1% NaCl (Merck Eurolabs, Germany) in deionised water is used as a solvent for the polymer as described in [6]. 0.1% formalin is added as oxygen scavenger. Polyacrylamide (Polysciences, $M_w = 1.8 \cdot 10^7 g/mol$) is added at a concentration of 80ppm. The shear-dependent viscosity of the polyacrylamide solution is determined with an AR2000 rheometer (TA Instruments). In figure 2 the dynamic viscosity η is plotted as a function of the shear rate $\dot{\gamma}$. It can be described with the Power-Law model $\eta(\dot{\gamma}) = K \cdot \dot{\gamma}^{n-1}$ with $K = 7.11 \cdot 10 - 3Pa \cdot s$ and $n = 0.976$. Therefore we also use the effective Reynoldsnumber $Re = \frac{\Omega_i \cdot r_i \cdot d \cdot \rho}{\eta(\dot{\gamma})}$ as a dimemsionless control parameter. It describes the ratio between inertia and viscous forces and is directly proportional to the angular velocity Ω_i of the inner cylinder. Respectively the effective Taylor number $Ta = Re\sqrt{d/r_i}$ is used.

Flow visualization

To visualize the flow structures with white light, we use Iriodin in $\Gamma = 10$ and Kalliroscope AQ1000 (Kalliroscope Corp., USA) in $\Gamma = 45.9$. An area scan CCD camera (Basler A641f, Basler AG, Germany) recordes the reflected light intensity along the axial direction

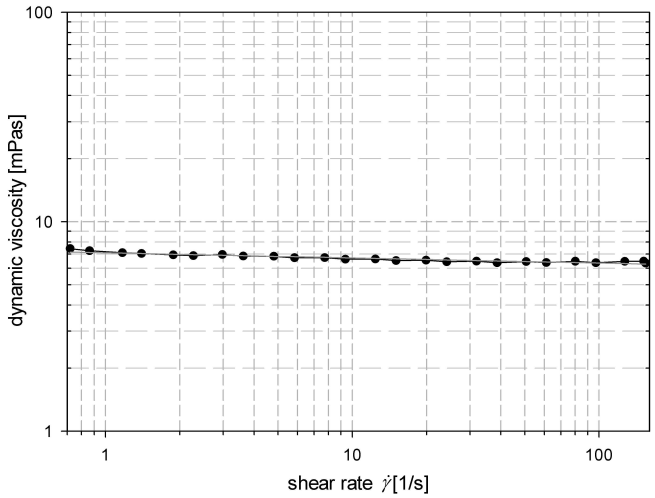

Figure 2: Shear-rate dependence of dynamic viscosity η of the polyacrylamide solution.

with 8-bit samplings in the large Taylor-Couette system. The camera is mounted with a lens f1.9/35mm. The spatial resolution amounts 4pixel/mm. In the small Taylor-Couette system we use a video camera (720x576 pixel, 26.8pixel/cm, 25frames/s) to record the fluid flow behaviour. From the recorded video sequences lines are extracted at $x = d/2$ from each frame. By chronological alignement of these lines, space-time diagrams are provided. The analysis of the space-time diagrams is based on a 2D Fourier analysis and complex demodulation. A detailed description of the procedure is given in [7], [9].

PIV system

To visualize the flow structures in the large Taylor-Couette system, hollow spheric glass particles with a diameter range $d_p = 8 - 11\mu m$ are used. The PIV system (MasterPIV) consists of a pulsed Nd:YAG laser (30mJ, $\lambda = 532nm$). A 8-bit CCD camera with sensor resolution 1034x779 pixel records the illuminated cross-section. The time delay between the two images of an image pair varies from 2.4 to 12ms, depending on the Taylor number, the time interval between the image pairs is 0.5s. The correlation of the images is calculated with Corélia-V2IP to obtain the 2-dimensional velocity field in r,z-plane. Therefore it is used the cross-correlation function. A schematic representation of Taylor-Couette system with PIV is given in figure 3.

To determine the velocity field in the small Taylor-Couette system ($\Gamma = 10$) a PIV system from TSI company is utilized. Polymer particles with a diameter range $d_p = 13 - 35\mu m$ are used to visualize the flow. A pulsed Nd:YAG laser (15mJ, $\lambda = 532nm$) combined with lightsheet optic illuminates the cross-section. A CCD camera with sensor resolution of 1024x1000 pixel is used for recording the pictures. The correlation of the images is calculated with the cross-correlation function with INSIGHT.

From the instantaneous 2D velocity fields lines at different positions in the cross-section are extracted. By chronological alignement space-time diagrams of $V_z(z,t)$ and $V_r(z,t)$ are provided. With 2D FFT analysis and complex demodulation the space-time diagrams are analysed, using a program developed by Abcha [12].

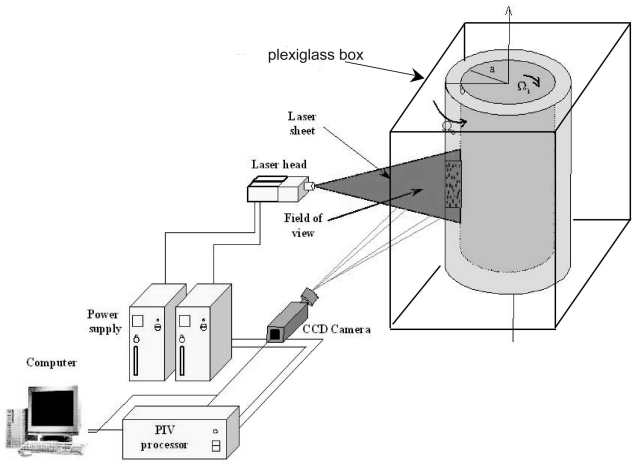

Figure 3: Schematic representation of PIV measurements in the Taylor-Couette system.

3 Results

In the small Taylor-Couette system ($\Gamma = 10$), one observe the transition from basic Couette flow to Taylor vortex flow. As for Newtonian fluid, Wavy vortex flow is observed at higher Taylor numbers. At further increase of rotation rate, the outflow between the vortices moves up and down whereas the inflow is stationary.
In the large aspect ratio Taylor-Couette system ($\Gamma = 45.9$) the observed behaviour differs from that at $\Gamma = 10$ and from results of Groisman and Steinberg [5] ($\eta = 0.708, \Gamma = 54$). We note a coexistence of various instabilities. In addition to Taylor vortices, Standing waves develop at the transition from circular Couette flow. This suggests, that the investigations are close to a codimension point. A periodic weak oscillation of Taylor vortices occurs in the lower part of the system at $\epsilon = (Ta - Ta_c)/Ta_c = 0.046$, which can be observed over a wide range of Taylor number. The onset of very weak oscillating rolls is at $\epsilon = 0.787$ in the middle of the Taylor-Couette system. Crumeyrolle et al. [8] described this instability as reduced amplitude WVF. Different to their observations we have not noted the WVF before the weak oscillating rolls appear.
In the large aspect ratio Taylor-Couette system PIV measurements are not done over the whole length of the system. Figure 4 displays the two different measurement positions.

Figure 5 displays the velocity field at the 2 different measurement positions. In A one observes periodic weak oscillating Taylor vortices. In contrast, at measurement position B, dynamic vortices in the transition zone between Taylor vortices on left side and Standing waves on right side exists. This dynamic vortices exhibit a GS mode: a wave component with a modulation appears, leading to a periodic flattening of the outflow boundary of the vortices [10, 11]. Figures 5 (d-f) display the axial and radial velocity components at both measurement positions. To determine the highest ranges of velocity inside the observed area, positive values correspond to red color, negative velocity values are blue.

In analogy to provide space-time diagrams from visualization experiments, the instantaneous velocity component $V_r(z,t)$ and $V_z(z,t)$ is extracted from PIV data (shown in figure 5 (d-g)) and aligned chronologically (figures 6,7). Red colors correspond to

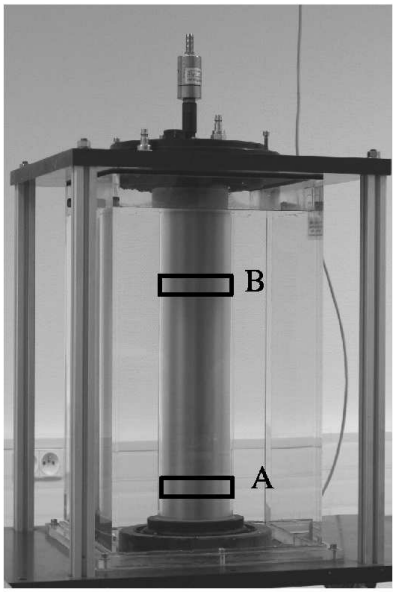

Figure 4: PIV measurement positions in the large Taylor-Couette system $\Gamma = 45.9$, $\eta = 0.8$.

positive values of the velocity and blue to negative one in the spatio-temporal plots.

In figure 8 the radial and axial velocity components at measurement position B for Ta=47 are shown. Compared with figure 7 the vortices shifted downward due to decrease of the number of Standing waves. Figure 9 shows a period of the flow structures at Ta=47 in position B. Between each pictures is a $\Delta t = 0.5099s$, so the period has the frequency $f = 0.3922Hz$.

4 Conclusion

Particle Image velocimetry is used to measure the velocity field in r,z plane in small and large aspect ratio Taylor-Couette systems. Space-time diagrams from axial ($V_z(z,t)$) and radial ($V_r(z,t)$) velocity component have been extracted and evaluated with 2D Fourier analysis and complex demodulation. A GS mode was observed in Taylor-Couette system with $\Gamma = 45.9$ in the transition zone between Taylor vortex flow and Standing waves.

Acknowledgements

This work is partially supported by a PhD fellowship from Brandenburg University of Technology Cottbus and the SOKRATES/Erasmus program. M. Smieszek would like to thank Innocent Mutabazi for the welcoming in the ITP team of the LMPG.

References

[1] Böhme G (2000): Strömungsmechanik nichtnewtonscher Fluide, 2nd Ed., Stuttgart, Teubner

[2] Pakdel P., McKinley G.H. (1997): Digital particle image velocimetry of viscoelastic fluids, *AIChE J*, **43**, 289-302

[3] Adrian R.J. (1991): Particle-imaging techniques for experimental fluid mechanics, *Annu. Rev. Fluid Mech.*, **23**, 261-304

[4] Baumert B.M., Liepmann, D., Muller, S.J. (1997): Digital particle image velocimetry in flows with nearly closed pathlines: the viscoelastic Taylor-Couette instability, *J. Non-Newt. Fluid Mech.*, **69**, 221-237

[5] Groisman A., Steinberg V.(1996): Couette-Taylor Flow in a Dilute Polymer Solution, *Phys. Rev. Lett.*, **77**, 1480-1483

[6] Groisman A., Steinberg V. (2000): Elastic turbulence in a polymer solution flow, *Nature*, **405**, 53-55

[7] Bot P., Mutabazi, I. (2000): Dynamics of spatio-temporal defects in the Taylor-Dean system, *Eur. Phys. J. B*, **13**, 141-155

[8] Crumeyrolle O., Mutabazi I., Grisel M. (2002): Experimental study of inertioelastic Couette-Taylor instability modes in dilute and semidilute polymer solutions, *Phys. Fluids*, **14**, 1681-1688

[9] Crumeyrolle O., Latrache N., Mutabazi)., Ezersky A. (2005): Instabilities with shear-thinning polymer solutions in the Couette-Taylor system, *J. Phys: Conf. Series*, **14**, 78-93

[10] Gorman M., Swinney H.L. (1979): Visual Observation of the Second Characteristic Mode in a Quasiperiodic Flow, *Phys. Rev. Lett.*, **43**, 1871-1876

[11] Takeda Y (1999): Quasi-periodic state and transition to turbulence in a rotating Couette system, *J. Fluid Mech.*, **389**, 81-99

[12] Abcha N., Latrache N., Dumouchel F., Mutabazi I. (2005): Application de la PIV pour la caractérisation du régime des rouleaux ondulés modulés dans le système de Couette Taylor, Colloque Franco-Tunisien Sur la Métrologie en Mécanique des Fluides, CFT'05, Monastir, Tunisie

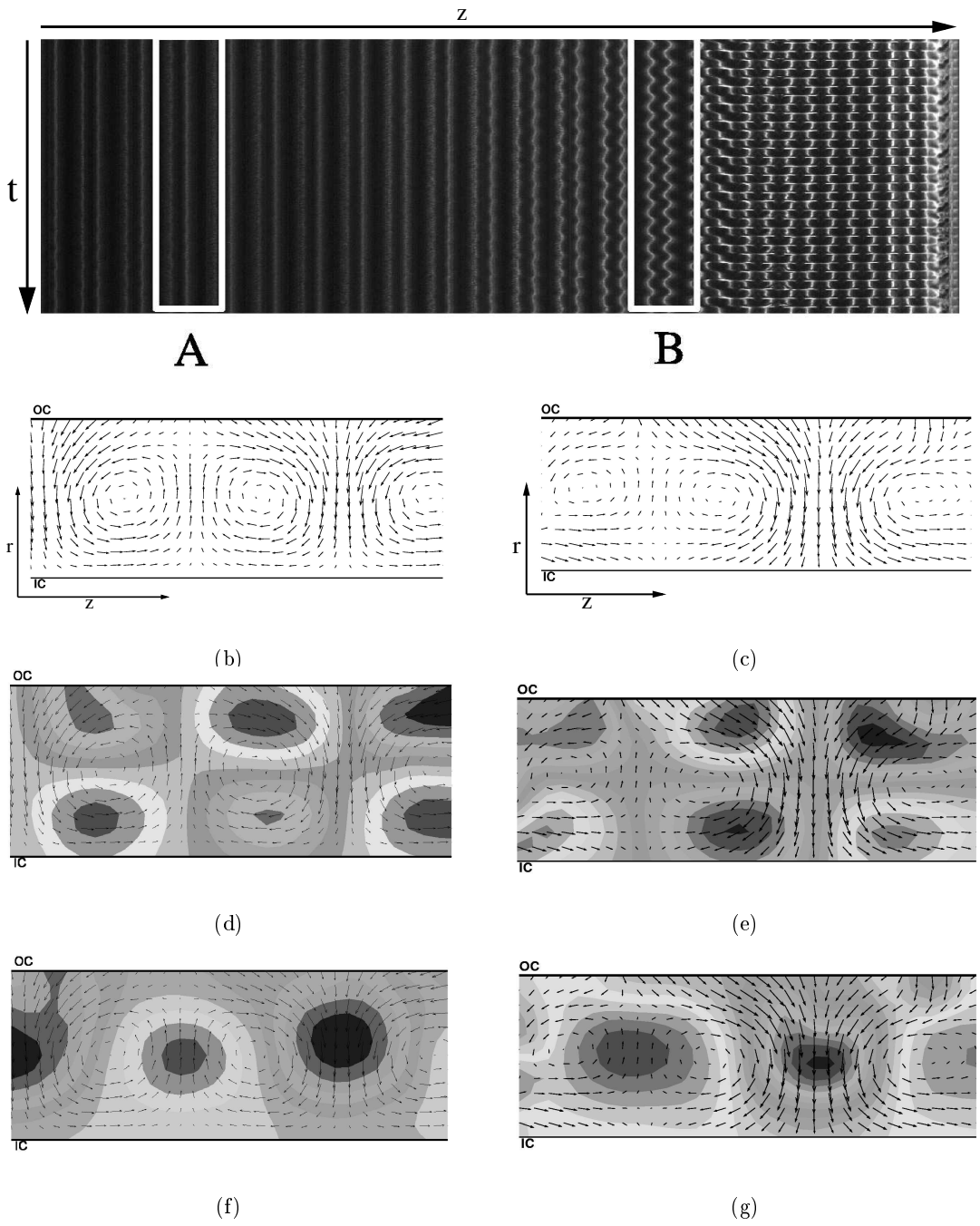

Figure 5: Velocity field from PIV measurements at $\Gamma = 45.9$, pos. A: Ta=41.7, pos. B: Ta=43.5. (a) Space-time plot from visualization with PIV measurement positions A and B, (b) velocity field (pos. A), (c) velocity field (pos. B), (d) axial velocity (pos. A), (e) axial velocity (pos. B), (f) radial velocity (pos. A), (g) radial velocity (pos. B), IC: inner cylinder, OC: outer cylinder

12.8

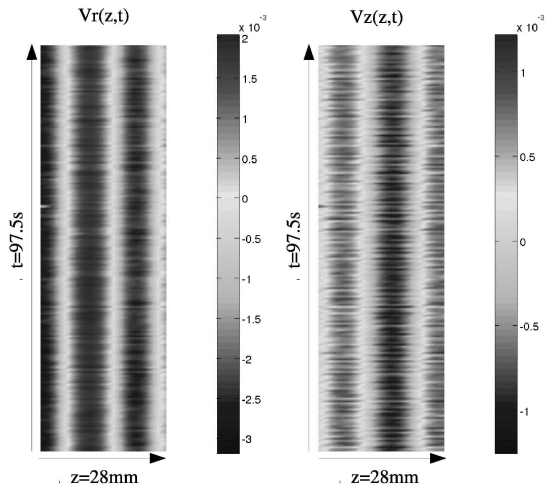

Figure 6: Space-time diagrams $V_r(z,t)$ and $V_z(z,t)$ for Ta=41.7 (measurement position A, $\Gamma = 45.9$)

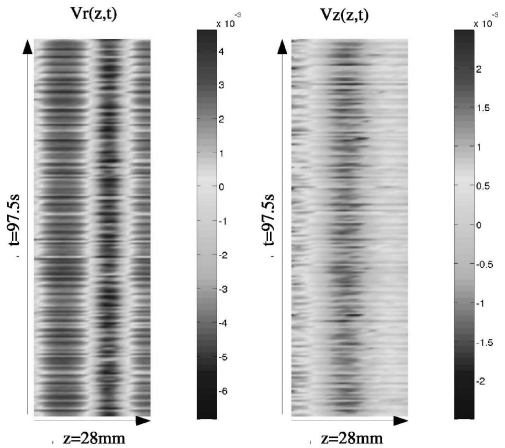

Figure 7: Space-time diagrams $V_r(z,t)$ and $V_z(z,t)$ for Ta=43.5 (measurement position B, $\Gamma = 45.9$)

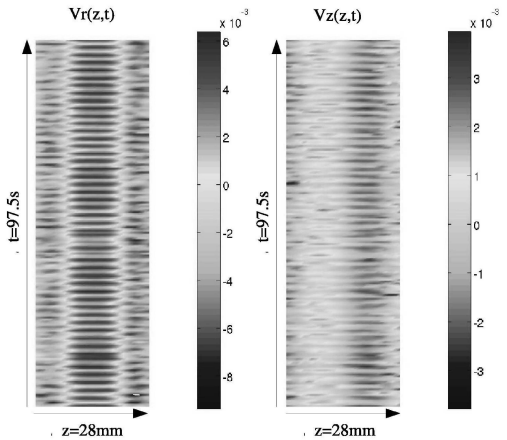

Figure 8: Space-time diagrams $V_r(z,t)$ and $V_z(z,t)$ for Ta=47 (measurement position B, $\Gamma = 45.9$)

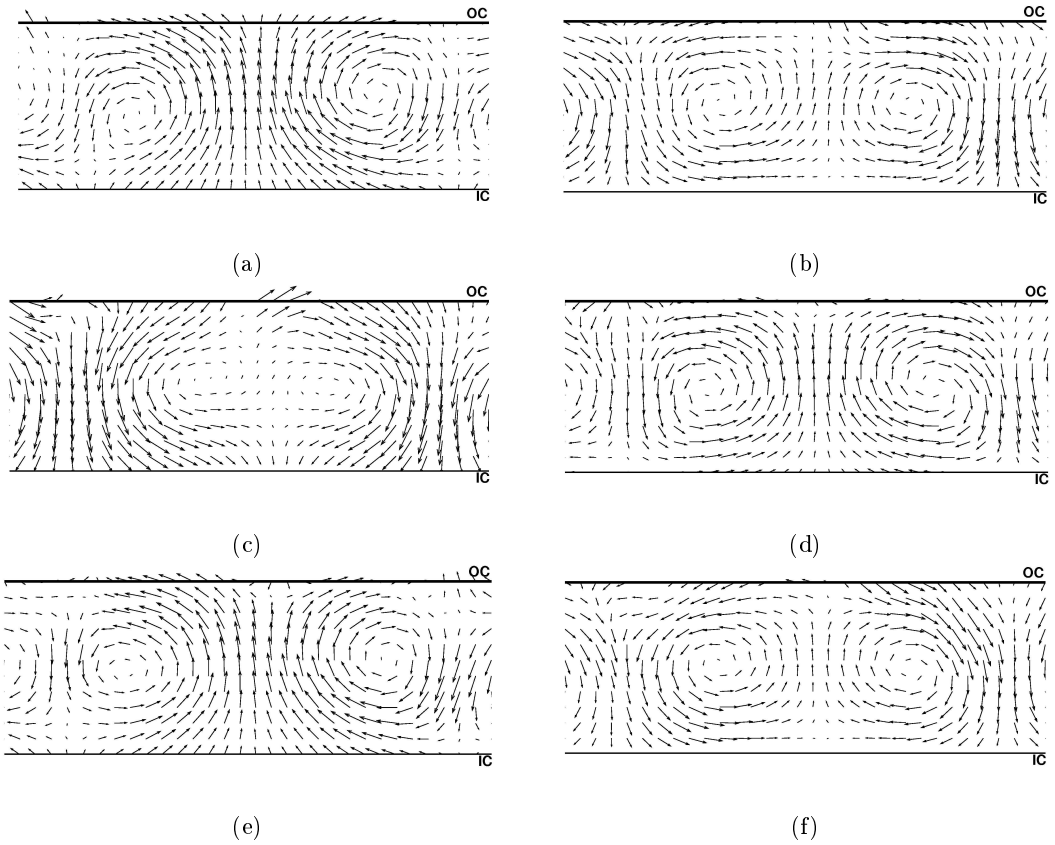

Figure 9: Velocity field for Ta=47 with $\Delta t = 0.5099s$ between each picture. (measurement position B, $\Gamma = 45.9$), IC: inner cylinder, OC: outer cylinder